J. Radiat. Res., 53, 101–109 (2012)

Experimental Model of Naturally Occurring Post-radiation Sarcoma: Interest of Positron Emission Tomography (PET) for Early Detection

Bérengère PHULPIN[1,2]*, Nguyen TRAN[3], Agnès LEROUX[2,4], Sylvain POUSSIER[5], Pierre-Yves MARIE[5], Sophie PINEL[2], Sandrine HUGER[6], Philippe HENROT[7], Patrice GALLET[2], Claire BLAISE[2], Pierre BRAVETTI[8], Pierre GRAFF[6], Jean-Louis MERLIN[2,4] and Gilles DOLIVET[1,2]

Rat model/Post-radiation sarcoma/MicroPET.

Radiotherapy is an integral part of overall cancer therapy. One of the most serious adverse effects of irradiation concern, for long-term survivors, the development of post-radiation sarcoma (PRS) in healthy tissues located within the irradiated area. PRS have bad prognosis and are often detected at a late stage. Therefore, it is obvious that the early detection PRS is a key-point and the development of preclinical models is worthy to evaluate innovative diagnostic and therapeutic procedures. The aim of this study was to develop a spontaneous murin model of PRS and to evaluate the potency of Positron Emission Tomography (PET) for early detection. Fifteen Wistars rats were irradiated unilateraly on the hindlimb with a single dose of 30 Gy. Sequential analysis was based on observational staging recordings, Computerized Tomography (CT) scanning and PET. Tumors were removed and, histopathological and immunochemistry analyses were performed. Among the irradiated rats, 12 sarcomas (80%) were detected. All tumors occurred naturallty within the irradiated hindlimb and were highly aggressive since most tumors (75%) were successfully transplanted and maintained by serial transplantation into nude mice. Upon serial staging recordings, using PET, was found to enable the detection of PRS earlier after irradiation than with the other methods (i.e. 11.9 ± 1.8 *vs* 12.9 ± 2.6 months). These results confirmed the interest of experimental models of PRS for the preclinical evaluation of innovative diagnostic strategies and confirmed the potency of PET for early detection of PRS. This preclinical model of PRS can also be proposed for the evaluation of therapeutic strategies.

INTRODUCTION

For decades, radiotherapy has been used extensively in the cancer treatment since nearly two thirds of all cancer patients have received radiotherapy at some point during their disease management.[1,2)] In addition, some recent salvage treatment procedures include reirradiation.[3)] The obvious success of this therapy, well established for instance in most early-stage cancers leading to long term survival, should not however hide from view the recurrent issues concerning late side-effects associated with ionizing radiations. One of the most serious adverse event feared for irradiation therapy is the late development of post-radiation sarcoma (PRS) in healthy tissues within the targeted irradiated area.[4)] The occurrence of PRS soft tissue sarcoma has been documented in a wide range of tissues including breast,[5–7)] ovarian,[6,7)] uterine,[6,7)] head and neck[5,8)] cancers as well as Hodgkin's and non-Hodgkin lymphoma.[5,7)] Other epidemiologic outcomes have pointed to a dramatically increase by 8–25 fold in the risk of development of PRS in breast and ovary.[7)] It is in keeping with the fact that other factors such as (i) the enhanced adverse exposure of healthy tissue to irradiation in case of use of intensity-modulated radiotherapy to target more precisely tumours and/or (ii) the improvement of the life expectancies of patients with early-stage cancer treated with radiation, could be also an attribute of the

*Corresponding author: Phone: (+33) 3.83.59.84.47,
Fax: (+33) 3.83.59.85.72,
E-mail: berengere-phulpin@orange.fr

[1]Head and Neck Surgery and Dental Units, Oncologic Surgery Department, Centre Alexis Vautrin, Avenue de Bourgogne, Brabois, 54511, Vandoeuvre-lès-Nancy, France; [2]EA4421 SIGReTO Nancy University, Faculty of Medicine, Avenue de la Forêt de Haye, 54500, Vandoeuvre-lès-Nancy, France; [3]School of Surgery, INSERM U961, Faculty of Medicine, Nancy University, Avenue de la Forêt de Haye, 54505, Vandoeuvre-lès-Nancy, France; [4]Pathology and Tumor Biology Department, Centre Alexis Vautrin, Avenue de Bourgogne, Brabois, 54511, Vandoeuvre-lès-Nancy, France; [5]INSERM U961, Faculty of Medicine, Nancy University, Avenue de la Forêt de Haye, 54505, Vandoeuvre-lès-Nancy, France; [6]Radiotherapy Department, Centre Alexis Vautrin, Avenue de Bourgogne, Brabois, 54511, Vandoeuvre-lès-Nancy, France; [7]Radiology Department, Centre Alexis Vautrin, Avenue de Bourgogne, Brabois, 54511, Vandoeuvre-lès-Nancy, France; [8]Oral Surgery Department, Faculty of Dentistry, Nancy University, 96 av Mal de Lattre de Tassigny BP.50208, 54004, Nancy, France.
doi:10.1269/jrr.11008

enhanced incidence of secondary malignancies.[1)]

However, although cares have been taken as a core part of surveillance necessary to succeed in the cancer management,[8)] diagnosis is often late.[8,9)] This delay in diagnosis has bad incidence because of the well demonstrated aggressiveness of PRS.[9)] The complexity in the metabolic/functional cascades of irradiated tissue and the still unknown timing of the occurrence of such an event contribute to hamper prediction of irradiation related secondary tumors in both clinical and preclinical studies.[7,8,10)]

Therefore, in this experimental study, the feasibility of using non invasive imaging techniques such as PET, CT-scan for the early detection of naturally occur is, i.e. non grafted, PRS was investigated. Post-radiation tumors were induced in Wistar rats after a hindlimb irradiation at a monodose of 30 Gy. Analyses were based on longitudinal imaging using CT-scan and 2-[18F]fluoro-2-deoxy-D-glucose (FDG)-PET scanning, and on observational staging recordings.[11)] Pathological, autoradiohistology and immunochemical analyses were performed additionally to characterize the tumor.

MATERIALS AND METHODS

Animals

This 15-month study was conducted in 15 male and adult Wistar rats (Janvier CERJ, Le Genest Saint Isle, France), weighting 440 ± 20 g at the beginning. All experimental procedures were in accordance with our local ethical committee and with the regulations of the Animal Welfare Act of the National Institute of Health Guide for the Care and Use of Laboratory Animals (NIH Publication No. 85-23, Revised 1996).

Irradiation procedures

Cobalt 60 irradiation was chosen to minimize the difference in the absorbed dose in soft and hard tissues. According to our experiences, a single dose of 30 Gy was delivered.[12)] Prior to irradiation, a scanner acquisition (Philips Brillance 40) enabled the calculation of dosimetry (Isogray 3.0 software Dosisoft). The room temperature during irradiation was 22°C. The animals, under general anaesthesia, were positioned in a prone and dorsal decubitus position upon a thick polystyrene phantom. The focus skin distance was 70 cm and the field size was 20 × 30 cm. The lead collimating block was positioned on a 0.5 cm thick acrylic plateform to shield the body and expose only the hindlimb without the pelvis. Radiation was then delivered, at a single dose of 30 Gy unilaterally on the right hindlimb, in a vertical beam from a Theratron® 780C X-ray machine (1.25 MeV). The irradiated volume was 40 cm^3 at a dose rate of 1.4 Gy/min.

Observational staging recordings

Rats were followed-up weekly. The recorded criteria for acute toxicity of irradiation were the appearance of alopecia and the irradiation-induced dermatitis. In addition, throughout the study, we studied the evolution of the weight curve and monitored the locomotion of animals.

Positron emission tomography

From the sixth month, FDG captation in hindlimb was performed every 30 to 45 days (depending to the availability of the PET scan facility) using a small animal positon emission tomography (MicroPET; Inveon Siemens Medical USA, Inc.). Animals were fasted overnight and anesthetised by inhalation of isoflurane (1.5% v/v) all along PET recording. FDG (74 MBq) was injected intravenously. Hindlimb PET was recorded 5 min after FDG injection and during a 60-min period, and it was followed by a 6-min transmission with a ^{57}Co point source recording in order to evaluate attenuation map and apply emission scatter correction during image reconstruction. Field of view was 12 cm, consequently the acquisition was centered on the hindlimb. PET was analyzed in all rats by the Inveon Research Workplace software (Siemens Medical USA, Inc.). Images were reconstructed in 6 frames of 10 min. Reconstruction process used a 3D OSEM algorithm with 4 iterations, 128*128 matrix, 1.0 zoom and 0.8 mm thickness, leading to a voxel size of $0.8 \times 0.8 \times 0.8$ mm. Images were corrected according to random coincidence counts, dead-time, activity decay, and for attenuation and scatter.[13,14)] In these conditions, the axial spatial resolution was less than 1.1 mm (1.1 mm of full width at half maximum for a point source placed at the centre of the field of view). Based on this, and since we only observed tumors of more than 2 mm of diameter, the problem of partial volume was not considered.

In order to normalize the differences in FDG uptake between the rats, SUV was calculated by measuring the radiopharmaceutical concentration within two-dimensional regions of interests (ROI) drawn around the leg. SUV was used to normalize radioactive counts from a particular ROI to the total dose injected and the body weight of the rats. The decrease of radioactivity was considered into Siemens® software. The standardized uptake values (SUVs) is defined by the formula:

$$\mathrm{SUV} = \frac{\text{tissue tracer specific activity (nCi/g)}}{\text{injected activity (nCi)/body weight (g)}}.$$

Active metabolic ROI was drawn based on SUV > 2.5 (using a cut-off value of 2.5) and regions of increased and abnormal FDG uptake higher than normal tissue uptake were characterized as tumor when SUV > 2.5.[15,16)] Similarly, the maximum standardized uptake value (SUVmax) was determined.

CT scan

From the sixth month, a CT scan was performed monthly concomitant with PET. The animals were anesthetized and positioned in dorsal decubitus. Since iodixanol has been reported to be rapidly excreted in rats with a plasma half-life

of 25 minutes,[17] a helical scanner acquisition (Philips Brillance 40) of the whole body (average acquisition field 290 mm) was immediately performed following the intravenous injection of 0.5 mL of iodoxanol (Visipaque, GE Healthcare®, Vélizy-Villacoublay France). CT scans were obtained with 150 mA and 120 kV. No triggering respiration was used. The mean acquisition time was 20 seconds. CT scan were reconstructed with a slice thicknesses of 0.9 mm and an increment of 0.4 mm. Each image file consisted of a 512 × 512 matrix of pixels. The opacity of each pixel was represented by a 16-bit gray-scale value. The CT scan was then reevaluated at the same interpretation session with the addition of soft tissue window (window level 80 HU, window width 280 HU) and a bone tissue window (window level 500, window width 1500 HU).

Histopathological and immunochemistry studies

After the development of the tumors the animals were sacrificed by injection of high doses of pentobarbital and KCl. The excised tumors, the lungs and the liver were immersion-fixed in AFA (acid acetic, formaldehyde, alcohol) for 24 hours and then embedded in paraffin. Five micrometer sections were stained with hematoxylin and eosin (HE) prior to light microscopic observations. Additional sections of the mass were stained immunohistochemically on Ventana Benchmark with the antibodies for vimentin (monoclonal mouse V9, 1:200, Dako Corporation, Trappes, France Corporation, Trappes, France), desmin (monoclonal mouse D33, 1:100, Dako Corporation, Trappes, France), actin (monoclonal mouse HHF35, 1:200, Dako Corporation, Trappes, France), S 100 protein (polyclonal rabbit, 1:1000; Dako Corporation, Trappes, France), cytokeratin AE1/E3 (monoclonal mouse AE1/AE3, 1:100, Dako Corporation, Trappes, France) and FVIII (polyclonal rabbit, 1:400, Dako Corporation, Trappes, France).

All microscope images (microscope Aristopla, Leica®), were captured with a camera (Olympus DP Controler, Olympus Optical) and analyzed with image analyzing software (TRIBVN-ics image communication software version 1.5, Chantillon France).

Microimager

In some animals, a piece of tumor was excised and snap-frozen in liquid-nitrogen cooled isopentane. A cryosection of 15 µm thick was performed and analyzed on a beta microimaging system (µIMAGER, Biospace, Paris, France), which allows recording of high resolution images, in order to highlight the captation of FDG. This imaging and counting system detects electrons emitted on the overall surface of histopathological slices with a high spatial resolution (20 µm).[18]

Then, this cryosection was stained with HE and an image of the all section was performed with a microscope (Axiocam, Carl ZEISS® Germany), equipped with software AxioVision (Carl ZEISS® Germany). A fusion of the µIMAGER and the HE images was obtained with the Photoshop CS software.

Tumor agressiveness

To assess tumor aggressiveness, serial grafting was performed. Each tumor was directly transplanted into 3 different 6-to 8-week-old, pathogen-free, athymic Ncr/Sed nude (nu/nu) mice (Charles River) as described.[19] When source tumors were excised, a piece was cleaned from necrotic tissue, cut into small chunks, and transplanted subcutaneously in each of the hindlimb of each mouse. Tumor aggressiveness was considered as positive when the tumors size exceeded 800 µm and could be serially transplanted at least 4 times.

RESULTS

Observational staging recordings

The weight of animals steadily increased (440 ± 20 g before irradiation, 519 ± 68 g at 6 months and 590 ± 79 g at 10 months after irradiation), consistently with the reference weight curve provided by the animal provider (463 ± 80 g at 6 months and 550 ± 92 g at 10 months).

No sign of evident impairment of locomotion was observed during the staging period.

All irradiated animals developed alopecia within the irradiated area. It became apparent in the irradiated hindlimb, 4 to 5 weeks after irradiation, and was irreversibly stabilized at 8–10 weeks. During sequential observation, two rats died during anesthesia 13-months after irradiation.

Macroscopically, all other rats excepted one (n = 12, 80%) developed a neoplasia which became detectable 12.9 ± 2.6-months after irradiation. All tumors were localised within the area of alopecia, either on the thigh (5 cases) or on the leg (7 cases). All the tumors were well circumscribed, located deep within the soft tissues and firm at palpation. In 6 cases, the tumors were located at the surface of the skin and were associated with a necrotic ulceration, surrounded by elevated and indurated borders. The expensive expansion of all the neoplasm at the time of the discovery and their high vascularisation, leading to considerable bleeding during the tumor removal, were additional supporting arguments for the establishment of the malignant nature.

Scanner staging

Despite the iodine injection, the opacity and the contrast uptake were insufficient to enable early detection of tumors. All tumors were detected later as they macroscopically invaded and distorted the surrounding soft tissue (Fig. 1).

No bone, lung or hepatic metastasis was detected even in the advanced cancers.

Positron emission tomography staging

Over the time, PET imaging revealed the tumors (Fig.

2A). All the early detected tumors were followed until they reached approximately 6 to 8 mm in diameter in order to be harvested and analysed using µIMAGER and histopathology. ROI were drawn (Fig. 2B), quantitative analyses were performed, and SUV and SUVmax were determined. The tumors were detected at 11.9 ± 1.8 months. We found that the development of a tumor was signed by a SUVmax > 2.5 and was further confirmed by histological analyses (see below). The SUVmax increased in a linear way to reach a plateau (Fig. 2C).

In 3 cases, the SUVmax was > 2.5 without being a tumor. The increased uptake was only detected on one PET for each rat, around the skin, and reached approximately 2.5 mm. As opposed to captation pattern observed in validated tumors (SUV > 2.5, persistent during time, located within soft tissues), in theses 3 cases the tumor captation was only super-

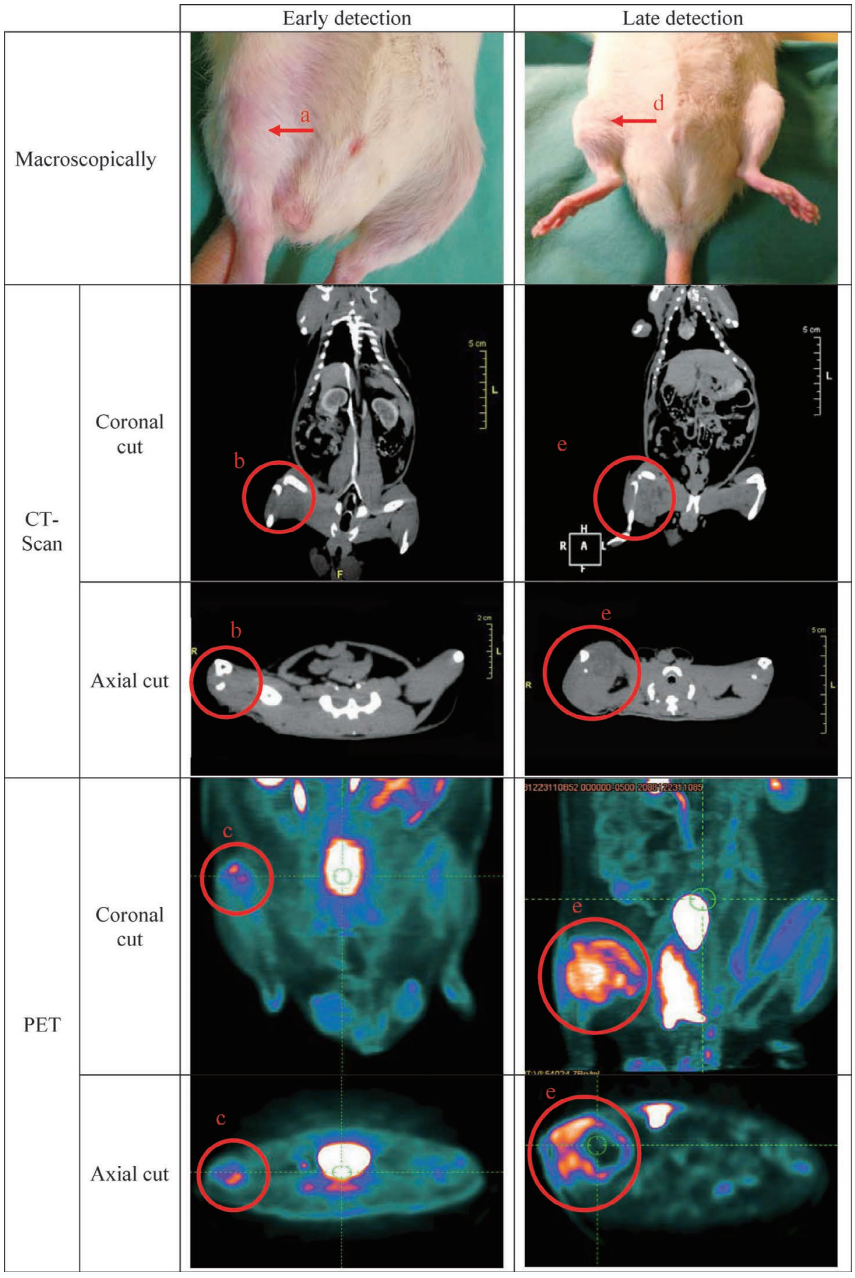

Fig. 1. Example of macroscopic images, PET and CT scan cuts performed on the same rats hindlimb 12 months and 14 months after 30 Gy irradiation. a: macroscopic view of alopecia within the irradiated area. b: no detectable tumor on axial and coronal cut. c: FDG uptake highlighting the tumor on both coronal and axial cuts. d: macroscopic view of hindlimb tumor. e: tumor invading and distorting the surrounding soft tissue.

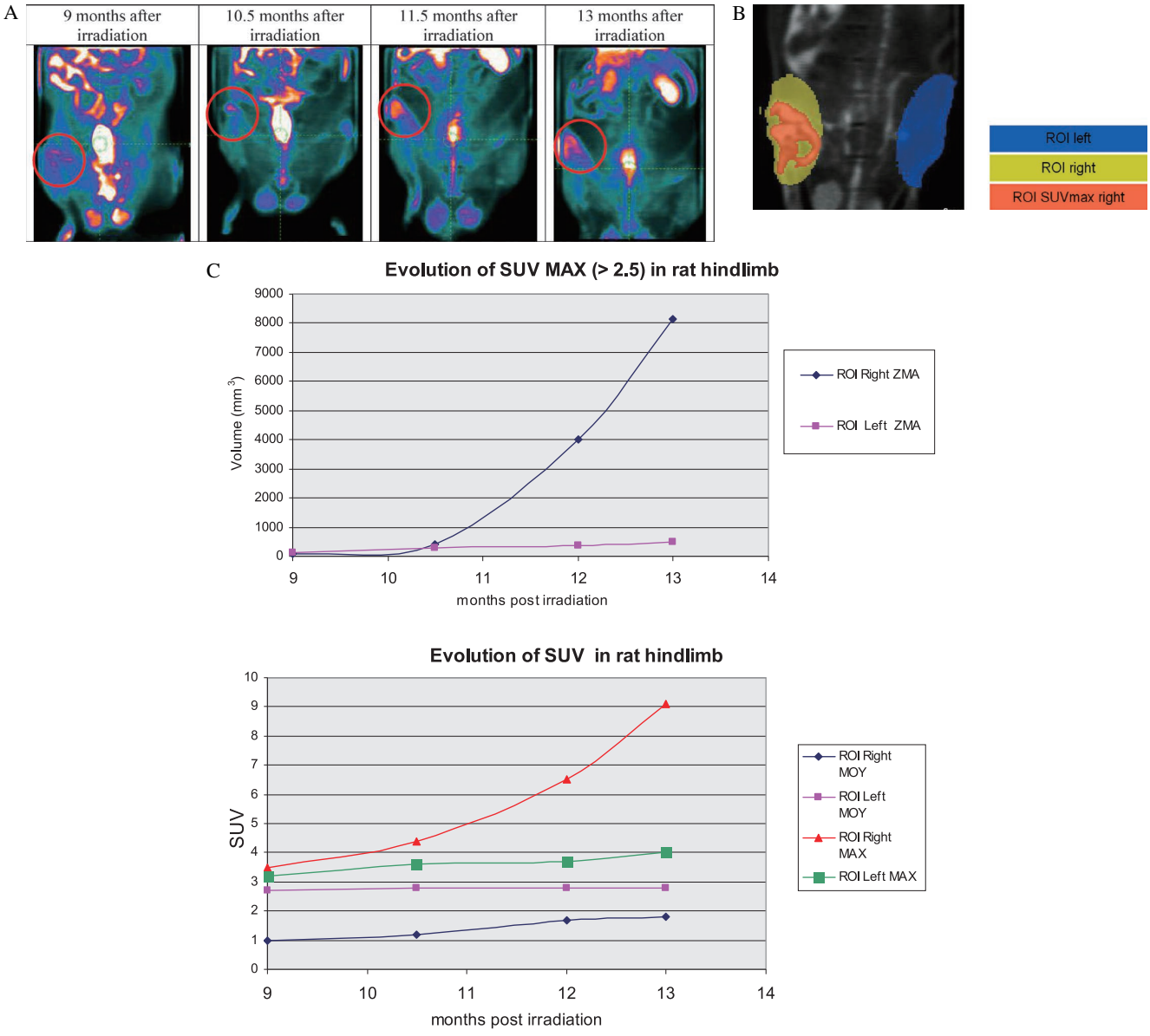

Fig. 2. Examples of PET images, ROI and evolution of SUV and SUVmax over the time. A: example of PET imaging revealing the tumor over the time. B: example of determination of the ROI SUV and determination of SUVmax on hindlimb. C: example of evolution of SUV and SUVmax over the time.

ficial and was not detected on the following PET and was consistent with a superficial temporary skin inflammation.

As in human imaging, the FDG captation was limited to the tumor and only a background captation was detected in the surrounding healthy tissues (Fig. 3). Regarding the medium SUV, we observed an increased uptake and sometimes stagnation in the uptake probably due to the presence of a zone of central necrosis intra-tumor. This was confirmed by the µIMAGER, whose images highlighted the absence of FDG in the necrotic areas (Fig. 3).

In some tumor detected by PET, a second PET was performed 10 days later. A visual contouring of the tumor periphery was performed on Siemens® software on the first and second PET to calculate tumor volume. In 10 days, tumor values increased by 1.6 fold.

Histological studies

No pulmonary or hepatic metastasis was found. All tumors were histologically characterized as sarcomas and confirmed by IHC since all tumors were diffusely positive for vimentin and negative for S 100 protein, cytokeratin AE1/E3 and FVIII.

Ten sarcomas were undifferentiated high grade sarcomas. The pleomorphic tumors infiltrated diffusely the skeletal

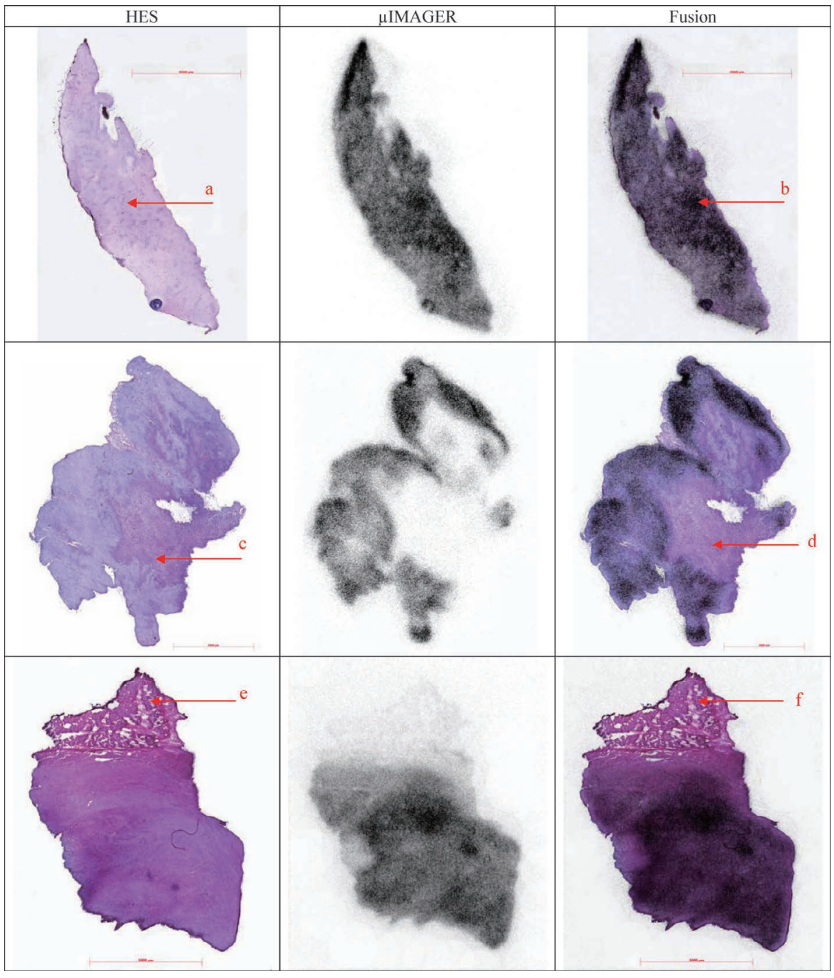

Fig. 3. Examples of HES and µIMAGER images of the same cut and fusion of these images. a: intratumoral area. b: FDG uptake throughout the tumor area. c: area of necrosis. d: absence of any uptake in the necrotic area. e: muscular area of healthy tissues. f: absence of any uptake in the muscular area of healthy tissues.

muscle fibers and cell overgrowth induced a localized loss of architecture with deep infiltrates. Histological observation revealed spindle cells focally arranged in a storiform growth pattern (Fig. 4). Spindle cells were mixed in 4 cases with multinucleated giant cells and in one case multinucleated giant cells were preponderant. The tumor cells appeared poorly differentiated with scanty eosinophilic cytoplasm, nuclear atypia with hyperchromatic and increased nuclei, and pleomorphism, mitotic activity was prominent (not shown). There was a little collagen in the matrix background. In all cases, IHC staining was negative for actin and desmin.

In one case, the tumor consist of spindle cells focally arranged in a herringbone growth pattern. Moreover, multinucleated giant cells were abundant and there was less collagen in the matrix background than in the previous tumors. The tumor was diffusely positively stained for vimentin and some spindle cells were positively stained for actin and desmin. This immunostaining pattern suggested that it was a sarcoma with a contingent of smooth muscle cell type leiomyosarcoma (Fig. 4).

In the last case, histological study of the leg neoplasm highlighted an osteosarcoma that produced osteid, consistent with osteoblastic sarcoma. IHC staining was negative for actin and desmin (Fig. 4).

Tumor agressiveness

Among the 12 tumors grafts, 3 failed at passage 1. The other tumors were very expansive, well circumscribed and firm at palpation. Histological studies performed showed that there was no change in histological types all along the 4 passages. Only slight morphologic differences were observed with an increase in cellular density and smaller and rounder shape of the cells than in the initial tumors.

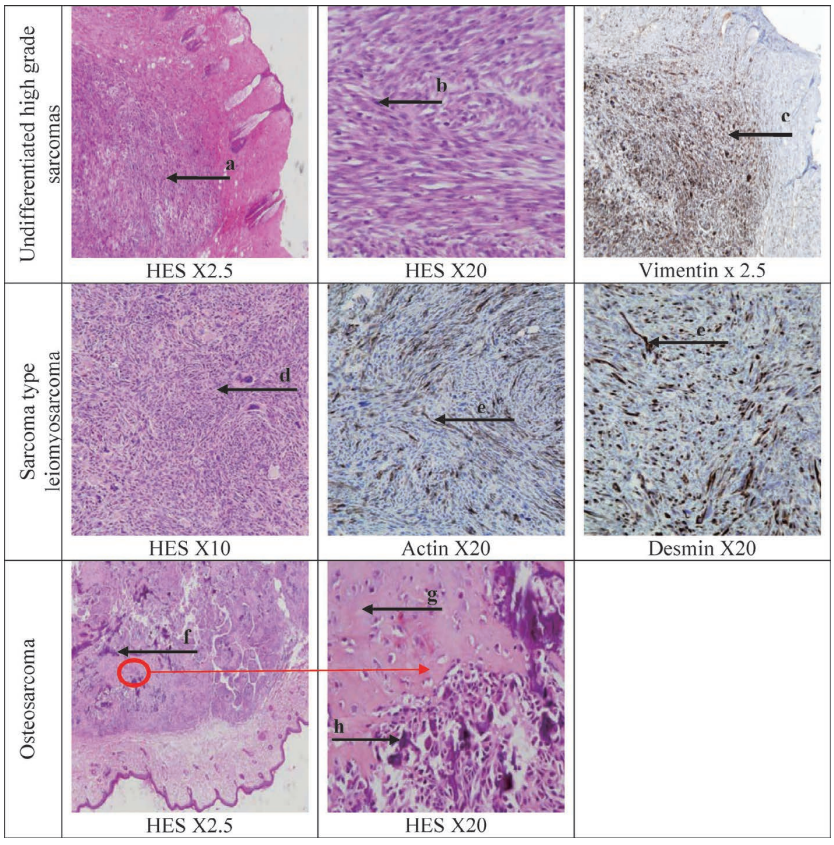

Fig. 4. Examples of micrographs taken from tumor tissues stained with HES and IHC. a: tumors infiltrated diffusely the skeletal muscle fibers. b: spindle cells focally arranged in a storiform growth pattern. c: tumor diffusely positive for vimentin. d: spindle cells focally arranged in a herringbone growth pattern. e: smooth muscle positively stained for actin and desmin. f: malignant bone formation by the tumor cells of osteosarcoma. g: osteoid tissue. h: very basophilic malignant bone.

DISCUSSION

One of the most serious side effects of radiotherapy, related to radiation-induced damage to normal cells is the induction of neoplasias.[20,21] In man, despites the well known risk[18] and advances in post-treatment survey and management, early diagnosis of these adverse events, probably compromised by the extremely versatile nature of post-radiation occurrence of tumors, is difficult. Hence, in animal models, little progress has been made, up to date, in quantifying such risks probably because of the lack of relevant models and of the difficulty of prediction or early diagnosis of such a late even. Therefore, global and comprehensive characterization of these particular tumors continues to be issued.

In the present long-term (> 12 months) study conducted in rats which experienced a monodose of 30 Gy in unilateral hindlimb, we documented an interesting high incidence of 80% of radiation induced soft tissue sarcomas according to current established criteria.[1,4] All sarcomas were located in the irradiated hindlimb. The occurrence of sarcoma has been already documented in murine models following irradiation but with a lower incidence.[22,23] In Sprague-Dawley rats after hindlimb fractionned irradiation with total cumulative doses of 46, 66, 86 or 106 Gy (delivered in 2 Gy fractions, each group receiving a final bolus dose of 16 Gy), Tinkey *et al.*[22] reported a total tumor incidence of 11% among which the most frequent tumor being osteosarcoma with a incidence of 17% after a cumulative dose of 106 Gy. More recently, Ando *et al.*[23] reported a total of 77 tumors in 371 mice that received γ-ray doses from 45 to 95 Gy. These authors identified malignant fibrous histiocytoma as the most observed tumor (60%), followed by carcinomas (25%). The reported low rate might be explained by the fact that doses accumulated over a period of time at low dose-rate would be biologically less effective than the same dose delivered in a single acute exposure.[24] Although the delivered dose was lower in our study, the observed higher incidence might be due to the different impact of unfractionated dose used. Furthermore, it has been showed that radiation might vary among the different strains of laboratory rats,[25] and Wistar rats might be probably more susceptible to radiation than

Sprague-Dawley rats as already suggested.[26] It is in keeping with the fact that spontaneous sarcoma is a very rare event in animals.[27] This high incidence of tumors makes our observation of sarcoma of particular interest, as it added to relatively few similar references in international literature.[22,23] We also succeeded to maintain the irradiation induced tumor during four serial transplantation, with no change in histological type, the tumors were very aggressive. After serial grafting, as the tumor line was established, the increase in cell density and modification in the cell morphology, seen in the immunocompromised recipient tissue, might suggest a higher degree in the aggressiveness of the tumors.

In this study, we challenged the early detection of radiation induced sarcomas by FDG-PET and CT-scan in small animal model. Small animal imaging has gained increasing attention in recent years as an excellent in vivo evaluation method in oncology research. In this particular model of late occurrence of radiation induced neoplasias, PET imaging might provide comprehensive representation of the extent and severity of metabolic/functional alteration within early cancer development.[11,28–31] Thus, evaluation of FDG uptake within a tumor was possible with the aid of CT images.[31] We are able in this study to show that PET and CT-scan images in rats were similar in quality to that observed in clinical oncology and thus the results achieved here clearly demonstrated the good quantitative ability of these imaging methodologies in rats. Accordingly, enhanced metabolic abnormalities of sarcomas were already documented by FDG-PET in the irradiated areas at 11.9 ± 1.8 months whereas CT-scan, which is the gold standard for the clinical detection of soft tissues sarcoma, and macroscopic visualization only evidenced tumors approximately one month later (i.e. 12.9 months after irradiation). The timing of the tumor occurrence compared satisfactorily with available data, a latency range of tumor induction being observed from a 4–25 month period.[22,23] In our study, as in humans, the threshold for tumor detection was set at SUVmax superior to 2.5.[32] It has been demonstrated that the metabolic parameters using SUVmax and metabolic tumor volume (TV) derived from TEP were positively correlated with T-stage in primary nasopharyngeal carcinoma patients.[33] Concerning the medium SUV, we observed an increased uptake and sometimes stagnation in the uptake probably due to the presence of a zone of central tumor necrosis. Similarly, in osteosarcoma, high SUVmax has been previously found to correspond to poor tumor necrosis on the histopathologic slab. As tumor necrosis is simply an estimation of the amount of viable tumor, SUVmax likely represents many viable tumor cells.[34] These sarcomas were poorly differentiated and very aggressive, as in human,[35] and we estimated the doubling time at 12.5 days. In this study, CT-scan seemed to be underpowered to detect early malignancies. The small size of the developing cancer and/or the sensibility of CT-scan used in our experiment might account for this discrepancy. However, it has been shown that FDG-PET was particularly helpful for the diagnosis in patients with suspected pancreatic cancer in whom CT-scan failed to identify a mass.[36] In this study, despite the injection of iodine, the contrast uptake of the tumors was insufficient for their detection. This can be explained by the low circulating blood volume of animals, limiting the volume of injection of the 270 mg I/ml iodoxanol for human use.

In a human case report of a post-radiation sarcoma with a very short latent period, serial diagnostic images were compared and revealed that FDG-PET was more potent than conventional imaging in distinguishing post-therapeutic change and tumor recurrence in the region after surgical and radiation therapy.[37] On the same way,[38] a patient who had been repeatedly treated for a peripheral nerve sarcoma, beneficed of a PET for the management of this disease. It showed regional recurrence, which required leg amputation. The pathological result has confirmed the PET diagnosis. PET was more potent than MRI to perform a differential diagnosis between postirradiation fibrosis and tumor recurrence, allowing for suitable therapeutic management of the patient.[38] Such information can be used to optimize staging, restaging, and assessment of response to therapy. Functional imaging with FDG-PET can also potentially help to better evaluate the patients prognosis both before and after neoadjuvant therapy.[28]

As more patients with early-stage cancer are treated with radiation and live longer, the incidence of post-radiation sarcomas is likely to increase as well. Therefore, the present preclinical model developed by a single dose 30 Gy irradiation of Wistar rat hindlimb, with a high incidence of soft tissue post-radiation sarcoma may be a useful animal model of naturally occurring post-radiation sarcoma suitable for the exploration of post-radiation sarcoma pathogenesis and evaluation of specific preventive or therapeutic approaches.

In this context, we report here that FDG-PET could be a reliable and useful imaging technique for early detection of post-radiation sarcomas.

ACKNOWLEDGMENTS

This works was granted by the French Ligue contre le cancer, Comités Lorrains and the Conseil Scientifique Nancyclotep, University Henri Poincaré Nancy.

REFERENCES

1. Cha C, *et al* (2004) Long-term results with resection of radiation-induced soft tissue sarcomas. Ann Surg **239**(6): 903–909; discussion 909–910.
2. Hogle WP (2006) The state of the art in radiation therapy. Semin Oncol Nurs **22**(4): 212–220.
3. Janot F, *et al* (2008) Randomized trial of postoperative reirradiation combined with chemotherapy after salvage surgery compared with salvage surgery alone in head and neck carci-

noma. J Clin Oncol **26**(34): 5518–5523.
4. Cahan WG, *et al* (1998) Sarcoma arising in irradiated bone: report of eleven cases. 1948. Cancer **82**(1): 8–34.
5. Sheppard DG and Libshitz HI (2001) Post-radiation sarcomas: a review of the clinical and imaging features in 63 cases. Clin Radiol **56**(1): 22–29.
6. Inoue YZ, *et al* (2000) Clinicopathologic features and treatment of postirradiation sarcoma of bone and soft tissue. J Surg Oncol **75**(1): 42–50.
7. Virtanen A, Pukkala E and Auvinen A (2006) Incidence of bone and soft tissue sarcoma after radiotherapy: a cohort study of 295, 712 Finnish cancer patients. Int J Cancer **118**(4): 1017–1021.
8. Maghami EG, *et al* (2005) Postirradiation sarcoma: a case report and current review. Am J Otolaryngol **26**(1): 71–74.
9. Robinson E, Neugut AI and Wylie P (1988) Clinical aspects of postirradiation sarcomas. J Natl Cancer Inst **80**(4): 233–240.
10. Sigurdson AJ and Jones IM (2003) Second cancers after radiotherapy: any evidence for radiation-induced genomic instability? Oncogene **22**(45): 7018–7027.
11. Riemann B, *et al* (2008) Small animal PET in preclinical studies: opportunities and challenges. Q J Nucl Med Mol Imaging **52**(3): 215–221.
12. Dolivet G (2009) Rehabilitation of irradiated tissues. Oncologie **11**(3): 526–527.
13. Kemp BJ, *et al* (2009) NEMA NU 2-2007 performance measurements of the Siemens Inveon preclinical small animal PET system. Phys Med Biol **54**(8): 2359–2376.
14. Visser EP, *et al* (2009) Spatial resolution and sensitivity of the Inveon small-animal PET scanner. J Nucl Med **50**(1): 139–147.
15. Hong R, *et al* (2007) Correlation of PET standard uptake value and CT window-level thresholds for target delineation in CT-based radiation treatment planning. Int J Radiat Oncol Biol Phys **67**(3): 720–726.
16. Lucignani G, Paganelli G and Bombardieri E (2004) The use of standardized uptake values for assessing FDG uptake with PET in oncology: a clinical perspective. Nucl Med Commun **25**(7): 651–656.
17. Heglund IF, *et al* (1995) Preclinical pharmacokinetics and general toxicology of iodixanol. Acta Radiol Suppl **399**: 69–82.
18. Mark RJ, *et al* (1994) Postirradiation sarcomas. A single-institution study and review of the literature. Cancer **73**(10): 2653–2662.
19. Pinel S, *et al* (2004) Erythropoietin-induced reduction of hypoxia before and during fractionated irradiation contributes to improvement of radioresponse in human glioma xenografts. Int J Radiat Oncol Biol Phys **59**(1): 250–259.
20. Fajardo LF (2005) The pathology of ionizing radiation as defined by morphologic patterns. Acta Oncol **44**(1): 13–22.
21. Fajardo LF (1986) Ionizing radiation and neoplasia. Monogr Pathol (27): 97–125.
22. Tinkey PT, *et al* (1998) Postirradiation sarcomas in Sprague-Dawley rats. Radiat Res **149**(4): 401–404.
23. Ando K, *et al* (2005) Tumor induction in mice locally irradiated with carbon ions: a retrospective analysis. J Radiat Res (Tokyo) **46**(2): 185–190.
24. Hall EJ (1991) Weiss lecture. The dose-rate factor in radiation biology. Int J Radiat Biol **59**(3): 595–610.
25. Suit H, *et al* (2007) Secondary carcinogenesis in patients treated with radiation: a review of data on radiation-induced cancers in human, non-human primate, canine and rodent subjects. Radiat Res **167**(1): 12–42.
26. Bartel-Friedrich S, Friedrich RE and Arps H (1999) Rat tumors following fractionated irradiation. Anticancer Res **19**(4A): 2725–2726.
27. Lavranos G, *et al* (2007) Casual discovery of a thoracic tumour showing histological features of undifferentiated pleomorphic sarcoma in a male Wistar laboratory rat. Anat Histol Embryol **36**(6): 433–436.
28. Bestic JM, Peterson JJ and Bancroft LW (2009) Use of FDG PET in staging, restaging, and assessment of therapy response in Ewing sarcoma. Radiographics **29**(5): 1487–1500.
29. Kumar R, *et al* (2006) Role of PET/PET-CT in the management of sarcomas. Expert Rev Anticancer Ther **6**(8): 1241–1250.
30. Wolf G and Abolmaali N (2009) Imaging tumour-bearing animals using clinical scanners. Int J Radiat Biol **85**(9): 752–762.
31. Tatsumi M, *et al* (2003) Initial experience in small animal tumor imaging with a clinical positron emission tomography/computed tomography scanner using 2-[F-18]fluoro-2-deoxy-D-glucose. Cancer Res **63**(19): 6252–6257.
32. Duysinx BC, *et al* (2006) 18F-FDG PET imaging in assessing exudative pleural effusions. Nucl Med Commun **27**(12): 971–976.
33. Chan WK, *et al* (2010) Nasopharyngeal carcinoma: relationship between 18F-FDG PET-CT maximum standardized uptake value, metabolic tumour volume and total lesion glycolysis and TNM classification. Nucl Med Commun **31**(3): 206–210.
34. Costelloe CM, *et al* (2009) Tumor necrosis in osteosarcoma: inclusion of the point of greatest metabolic activity from F-18 FDG PET/CT in the histopathologic analysis. Skeletal Radiol: 131–140.
35. Souba WW, *et al* (1986) Radiation-induced sarcomas of the chest wall. Cancer **57**(3): 610–615.
36. Delbeke D and Pinson CW (2004) Pancreatic tumors: role of imaging in the diagnosis, staging, and treatment. J Hepatobiliary Pancreat Surg **11**(1): 4–10.
37. Hsieh TC, *et al* (2009) Fulminant postirradiation soft tissue sarcoma. Clin Nucl Med **34**(11): 811–814.
38. Santaella Y, *et al* (2005) [18-FDG-PET in a case of recurrent malignant schwannoma]. Rev Esp Med Nucl **24**(2): 127–130.

Received on January 28, 2011
Accepted on April 4, 2011